Original Article

Value of dynamic contrast-enhanced ultrasound in predicting cervical lymph node metastasis in papillary thyroid carcinoma patients with Hashimoto's thyroiditis

Kairen Zhang, Dan Zhao, Ying Song, Xiaofeng Wu, Chenyang Jin, Fenglin Dong

Department of Ultrasound, The First Affiliated Hospital of Soochow University, Suzhou, China

Contributions: (I) Conception and design: K Zhang, F Dong; (II) Administrative support: X Wu, F Dong; (III) Provision of study materials or patients: D Zhao, C Jin; (IV) Collection and assembly of data: K Zhang, Y Song; (V) Data analysis and interpretation: K Zhang; (VI) Manuscript writing: All authors; (VII) Final approval of manuscript: All authors.

Correspondence to: Fenglin Dong, MD. Department of Ultrasound, The First Affiliated Hospital of Soochow University, 899 Pinghai Road, Suzhou 215031, China. Email: fldong@suda.edu.cn.

Background: Hashimoto's thyroiditis (HT) and papillary thyroid carcinoma (PTC) commonly coexist. An accurate assessment of cervical lymph node metastasis (CLNM) is crucial for determining treatment options and predicting prognosis. However, traditional examination methods have certain limitations. This study aimed to investigate the potential utility of dynamic contrast-enhanced ultrasound (DCE-US) using VueBox® software in assessing CLNM in patients with PTC coexisting with HT.

Methods: A retrospective analysis was performed on the clinicopathological data and ultrasound characteristics of 180 thyroid cancer patients who underwent either biopsy or surgery from January 2022 to November 2023. The dataset was partitioned into training and validation sets with a 6:4 ratio. Statistical analyses, including *t*-tests, chi-squared tests, and rank-sum tests, were conducted to evaluate the data. Univariate analysis, least absolute shrinkage and selection operator (LASSO) regression, and multivariate logistic regression were employed to identify the predictive factors for CLNM. Based on these analyses, three predictive models were developed: Model 1, incorporating clinical factors; Model 2, integrating clinical and ultrasound factors; and Model 3, a combined model that included both clinical and ultrasound factors using DCE-US. The diagnostic performance of each model was assessed using receiver operating characteristic (ROC) curves, calibration curves, and decision curve analysis (DCA).

Results: The Model 3 exhibited superior performance compared to Models 1 and 2. Specifically, in the training set, Model 3 achieved an area under the curve (AUC) value of 0.924 [95% confidence interval (CI): 0.857–0.966], and in the validation set, the AUC value was 0.905 (95% CI: 0.813–0.962). These values were significantly higher ($P<0.05$) than those of Model 1, which had a training AUC of 0.724 (95% CI: 0.630–0.806) and a validation AUC of 0.677 (95% CI: 0.557–0.783), as well as Model 2, with a training AUC of 0.854 (95% CI: 0.773–0.915) and a validation AUC of 0.797 (95% CI: 0.683–0.883). Moreover, DCA indicated that Model 3 provided a greater net benefit than Models 1 and 2 in both the training and validation cohorts.

Conclusions: The use of VueBox® perfusion analysis in DCE-US provides additional value in predicting CLNM in PTC patients with HT. The integrated model, which combines clinical and ultrasound factors, is a valuable diagnostic tool.

Keywords: Thyroid cancer; Hashimoto's thyroiditis (HT); lymph node metastasis; contrast-enhanced ultrasound (CEUS); nomograms

Submitted Nov 24, 2024. Accepted for publication Mar 07, 2025. This article was updated on Jul 01, 2025. The original version is available at: https://dx.doi.org/10.21037/gs-2024-510

doi: 10.21037/gs-2024-510

Introduction

Hashimoto's thyroiditis (HT), the predominant etiology of hypothyroidism, is an autoimmune condition characterized by extensive lymphocytic infiltration and persistent inflammatory responses, which may lead to chronic inflammation and thyroid dysfunction. Patients with HT often have a high prevalence of papillary thyroid carcinoma (PTC) with lymph node features like those observed in PTC metastases (1-3). Thus, the presence of HT in PTC cases may exacerbate the preoperative detection of cervical lymph node metastasis (CLNM) (4). Conventional ultrasound techniques exhibit less than 50% sensitivity in identifying metastatic cervical nodes in patients with PTC (5,6), and there are few studies on the impact of HT on ultrasound assessment for CLNM in PTC (3). The choice of surgical approach is directly influenced by the presence or absence of CLNM. Accurately evaluating CLNM before surgery is crucial for establishing the appropriate extent of lymph node dissection (7). Studies have demonstrated that patients with PTC and HT exhibit a reduced occurrence of CLNM compared to those with PTC exclusively (8,9). Nonetheless, PTC patients with HT who undergo surgical intervention typically have a greater number of lymph nodes excised, resulting in an increased incidence of comorbidities such as recurrent laryngeal nerve damage and hypoparathyroidism (10,11). Consequently, enhancing CLNM assessment in patients with PTC and HT is essential for improving patient outcomes.

In recent years, significant advancements have been made in contrast-enhanced ultrasound (CEUS) technology (12). Compared to color Doppler imaging, CEUS exhibits superior sensitivity to blood vessels and has been proven effective in differentiating between malignant and benign thyroid nodules (TNs) (13,14). However, the diagnostic potential of ultrasound imaging is often limited by the restricted ultrasound features discernible to the human eye, which constrains its widespread application as a diagnostic tool in clinical practice. Some researchers have evaluated the biological behavior of PTC with CLNM in association with its ultrasound features.

Dynamic contrast-enhanced ultrasound (DCE-US) is a quantitative imaging method that builds on CEUS images to derive reproducible perfusion parameters, thereby assessing TN microvascular perfusion dynamics (15). This technique facilitates easier interpretation and application, regardless of the operator's experience level (16,17). DCE-US has been used to determine the perfusion characteristics of thyroid adenomas and carcinomas (18). However, there is limited research on the efficacy of DCE-US in identifying metastatic CLNM from PTC in patients with HT. The integration of clinical information with DCE-US may enhance its diagnostic performance. Consequently, this study aimed to develop and validate a nomogram model that integrates clinical ultrasound data and DCE-US to predict CLNM in this population. We present this article in accordance with the TRIPOD reporting checklist (available at https://gs.amegroups.com/article/view/10.21037/gs-2024-510/rc).

Highlight box

Key findings

- The use of VueBox® perfusion analysis in dynamic contrast-enhanced ultrasound (DCE-US) provides additional value in predict cervical lymph node metastasis (CLNM) in papillary thyroid carcinoma (PTC) patients with Hashimoto's thyroiditis (HT).

What is known and what is new?

- Diagnosing PTC patients with HT at risk of CLNM is difficult. Contrast-enhanced ultrasound (CEUS) technology often rely on individual evaluations, while prognosis is affected by unobservable factors.
- The predictive model integrates DCE-US to visualize nodule perfusion. Quantitative parameters from these curves provide objective data on blood perfusion and washout, making it easier for operators to evaluate, making the model beneficial in clinical practice.

What is the implication, and what should change now?

- The utilization of VueBox® perfusion analysis to extract ultrasound parameters from DCE-US images offers a tangible benefit in predicting CLNM in patients with PTC and HT, potentially informing novel treatment strategies.
- Further research is warranted on DCE-US for the identification of metastatic CLNM in PTC patients with HT. This should include large-scale studies focusing on nodule perfusion and the optimization of its integration with DCE-US and other diagnostic modalities to enhance the accuracy of thyroid nodule diagnosis.

Methods

Our study retrospectively examined patients diagnosed with malignant TNs who were treated at The First Affiliated Hospital of Soochow University between January 2022 and December 2023. The study was conducted in accordance with the Declaration of Helsinki (as revised in 2013). The First Affiliated Hospital of Soochow University granted approval for this study (No. 2025227). Owing to the retrospective nature of the study, the requirement for

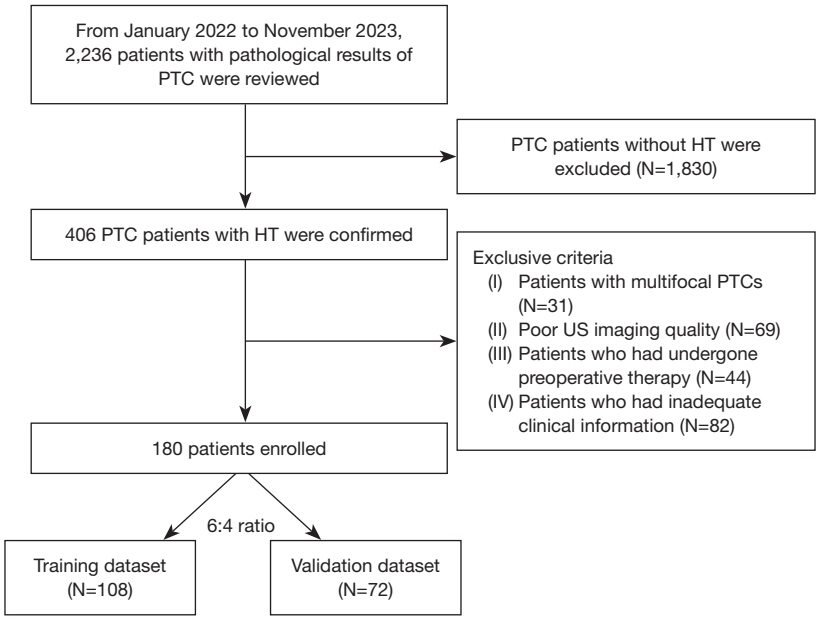

Figure 1 Flow chart of the study selection process. HT, Hashimoto's thyroiditis; PTC, papillary thyroid carcinoma; US, ultrasound.

informed consent was waived.

Participants were selected according to the following criteria: (I) existence of solitary-focus PTC; (II) postoperative histopathological confirmation of PTC accompanied by HT; (III) provision of unambiguous thyroid B-mode ultrasound (BMUS) images; and (IV) comprehensive clinical data, including patient demographics, ultrasound characteristics, thyroid function parameters [including total triiodothyronine (TT3), free triiodothyronine (FT3), total thyroxine (TT4), free thyroxine (FT4), thyroid-stimulating hormone (TSH), thyroid peroxidase antibody (TPO-Ab), thyroglobulin antibody (TG-Ab), and thyrotropin receptor antibody (TR-Ab)]. The exclusion criteria were as follows: (I) multifocal PTC; (II) substandard quality ultrasound imaging; (III) individuals who had received preoperative interventions, such as radiofrequency or microwave ablation, and (IV) patients with inadequate clinical data. *Figure 1* illustrates the detailed selection process. Ultimately, a total of 180 patients were included in the study. These patients were randomly assigned to either the training set (n=108) or the validation set (n=72) following a 6:4 ratio.

BMUS and CEUS procedure

The examinations were conducted by two radiologists with over 15 years of expertise in CEUS thyroid imaging, utilizing either the Mindray Resona7 or Resona9 ultrasound devices equipped with high-frequency linear array probes. Patients were positioned supine with their arms abducted to ensure adequate exposure of the thyroid. Initial grayscale ultrasonography examinations were performed, with documentation of the largest segments. Following this, 1.2–2.4 mL of sulfur hexafluoride microbubbles (Sono Vue®; Bracco, Milan, Italy) were administered, followed by a 5 mL normal saline flush. The timer and dynamic storage functions were activated simultaneously with the injection of the contrast agent. The probe was held in a fixed position for 2 minutes to capture the thyroid lesion in its maximal plane. The CEUS footage was archived in DICOM format as a cine loop, allowing for the recording and analysis of the nodules' strength. For conclusive analysis, a single frame depicting the maximum contrast intensity of the lesion during CEUS was selected.

Nodules were categorized according to the 2020 Chinese Thyroid Image Reporting and Data System classification (19). Two radiologists with over 15 years of experience in thyroid ultrasound image assessment retrospectively evaluated the ultrasound features without knowledge of the patients' clinical data. In cases of disagreement regarding the conventional ultrasound and CEUS features, a third radiologist reviewed the images to reach a consensus. The BMUS features assessed included lesion size (maximal diameter on BMUS), composition (cystic or almost completely cystic, solid, or almost completely solid),

echogenicity (isoechoic, hyperechoic, hypoechoic relative to adjacent thyroid parenchyma, or markedly hypoechoic), shape (wider-than-tall, taller-than-wide), margin (smooth, ill-defined, or irregular), extrathyroidal extension (ETE) (yes, no), and echogenic foci (none, comet-tail artifacts, punctate echogenic foci of uncertain significance, microcalcifications, or macrocalcifications).

For CEUS, each nodule's enhancement direction (scattered, centripetal, or centrifugal), enhancement pattern (homogeneous or heterogeneous), peak intensity (non-enhancement, hypo-enhancement, iso-enhancement, or hyper-enhancement relative to adjacent thyroid parenchyma at peak), and enhancement defects (absent or present) were recorded.

DCE-US analysis

CEUS data in DICOM format were imported into the VueBox software for offline analysis using the GI-Perfusion tool. A radiologist with a decade of expertise in thyroid CEUS, without knowledge of the patients' clinical, imaging, and pathological results, analyzed the digitally archived DICOM cine loops. CEUS clips were subjected to dynamic observations. For each nodule, two regions of interest (ROIs) were selected based on the greatest visual enhancement: a boundary ROI that included the nodule and adjacent thyroid tissue, and an analysis ROI that encompassed the area of maximal enhancement while excluding major vasculature or necrotic regions. Time-intensity curves (TICs) were generated and linearized to illustrate the average intensity in the ROIs over time, reflecting the movement of the contrast microbubbles. The following quantitative parameters were derived from the TIC: peak enhancement (PE), rise time (RT), time to peak (TTP), mean transit time local (mTTl), fall time (FT), wash-in area under the curve (WiAUC), wash-in perfusion index (WiPI), wash-in rate (WiR), wash-out area under the curve (WoAUC), combined wash-in and wash-out area under the curve (WiWoAUC), and wash-out rate (WoR). The fit quality between the echo-power signal and f(t) should be ≥75% (20). Respiratory compensation adjustments were implemented on curves that were substantially influenced by respiration to guarantee parameter reliability.

Statistical analysis

Statistical analyses were conducted using R (version 3.6.1), SPSS (version 27.0), and MedCalc (version 20.027). The Mann-Whitney *U* test or Student's *t*-test (for normally distributed variables) was used to compare quantitative parameters. In contrast, the chi-squared test was applied to categorical data and rates. To perform univariate analysis, *t*-tests, non-parametric tests, and chi-squared tests were utilized. Following this, multivariable logistic regression analysis was applied to create models for predicting CLNM in PTC with HT, using variables identified through the least absolute shrinkage and selection operator (LASSO) regression model. Receiver operating characteristic (ROC) curves were then generated to determine the cutoff value and Youden index. The DeLong test was used to assess the variations in the area under the curve (AUC) among the three models in the training and validation cohorts. A nomogram was created using multivariate logistic regression. Calibration curves and decision curve analyses (DCAs) were used to evaluate the validity and clinical effectiveness of the nomogram, respectively. The threshold for statistical significance was set at a two-sided P value of less than 0.05.

Results

Patient characteristics

This study enrolled 180 patients with a mean age of 41.88 years, including those diagnosed with PTC with and without CLNM. The training set consisted of 32 patients with CLNM and 76 patients without CLNM, whereas the validation set included 22 patients with CLNM and 50 patients without CLNM. The baseline characteristics of the training and validation sets were well-balanced (Table S1).

Model construction

The optimal cutoff points were determined using the Mean Line, PE, Wi AUC, RT, mTTl, TTP, WiR, Wi PI, Wo AUC, Wi Wo AUC, FT, Wo R, and Area values corresponding to the maximum of the Youden index. The cutoff values for these metrics are listed in *Table 1*. The univariate analysis of the training set indicated that TG-Ab, TR-Ab, Echogenic foci, ETE, lesion size, enhancement defects, Mean Line, Wi AUC, WiR, mTTl, Wi PI, Wo AUC, Wi Wo AUC, Wo R, and Area were substantially correlated with positive LNM (P<0.05), as presented in *Table 2*. A LASSO regression analysis was performed for further feature selection utilizing 10-fold cross-validation, resulting in the retention of eight features with non-zero

Table 1 Results of the univariate analysis of the training set

Variables	NCLNM (n=76)	CLNM (n=32)	Statistic	P
Area (cm^2)	0.60±0.70	0.94±0.77	t=−2.21	0.03
TT3 (ng/mL)	1.12±0.39	1.29±1.10	t=−1.13	0.26
FT3 (ng/mL)	4.68±2.43	5.73±7.37	t=−1.12	0.27
TT4 (ng/mL)	8.53±2.22	9.11±4.12	t=−0.75	0.46
FT4 (ng/mL)	40.93±221.37	18.80±17.56	t=0.56	0.58
TSH (uIU/mL)	4.97±20.72	8.02±24.47	t=−0.66	0.51
Lesion size (mm)	9.25±4.36	12.81±5.92	t=−3.07	0.004
Age (years)	41.18±11.33	41.88±11.69	t=−0.29	0.78
TPO-Ab (IU/mL)			χ^2=0.05	0.83
≤34	35 (46.05)	14 (43.75)		
>34	41 (53.95)	18 (56.25)		
TG-Ab (IU/mL)			χ^2=8.27	0.004
≤60	34 (44.74)	5 (15.62)		
>60	42 (55.26)	27 (84.38)		
TR-Ab (IU/mL)			χ^2=8.03	0.005
≤1.75	53 (69.74)	13 (40.62)		
>1.75	23 (30.26)	19 (59.38)		
Sex			χ^2=0.18	0.68
Male	8 (10.53)	5 (15.62)		
Female	68 (89.47)	27 (84.38)		
Echogenic foci			χ^2=9.76	0.008
None, comet-tail artifacts or punctate echogenic foci of uncertain significance	24 (31.58)	2 (6.25)		
Microcalcification	41 (53.95)	27 (84.38)		
Macrocalcification	11 (14.47)	3 (9.38)		
Echogenicity			–	0.37
Isoechoic	3 (3.95)	0 (0.00)		
Hypoechoic	67 (88.16)	32 (100.00)		
Hyperechoic	2 (2.63)	0 (0.00)		
Markedly hypoechoic	4 (5.26)	0 (0.00)		
Composition			–	0.69
Cystic or almost completely cystic	3 (3.95)	0 (0.00)		
Solid or almost completely solid	73 (96.0.6)	32 (100.00)		
Margin			χ^2=0.32	0.57
Smooth	18 (23.68)	6 (18.75)		
Ill-defined or irregular	58 (76.32)	26 (81.25)		

Table 1 (*continued*)

Table 1 (*continued*)

Variables	NCLNM (n=76)	CLNM (n=32)	Statistic	P
Shape			χ^2=1.61	0.20
Wider-than-tall	28 (36.84)	16 (50.00)		
Taller-than-wide	48 (63.16)	16 (50.00)		
Location			χ^2=3.74	0.15
Right	43 (56.58)	12 (37.50)		
Left	22 (28.95)	15 (46.88)		
Isthmus	11 (14.47)	5 (15.62)		
CDFI			χ^2=2.51	0.28
0	23 (30.26)	5 (15.62)		
1	43 (56.58)	22 (68.75)		
2	10 (13.16)	5 (15.62)		
ETE			χ^2=12.19	<0.001
No	66 (86.84)	18 (56.25)		
Yes	10 (13.16)	14 (43.75)		
Enhancement type			–	0.22
None or iso-enhancement	24 (31.58)	7 (21.88)		
Hypoenhancement	52 (68.42)	24 (75.00)		
Hyperenhancement	0 (0.00)	1 (3.12)		
Enhancement homogeneity			χ^2=0.20	0.65
Homogeneous	66 (86.84)	26 (81.25)		
Heterogeneous	10 (13.16)	6 (18.75)		
Filling defects			χ^2=14.73	<0.001
Absent	69 (90.79)	19 (59.38)		
Present	7 (9.21)	13 (40.62)		
Enhancement direction			χ^2=1.52	0.22
Scattered	23 (30.26)	6 (18.75)		
Centripetal or centrifugal	53 (69.74)	26 (81.25)		
Mean Line (au)			χ^2=4.05	0.04
>66,054.70	11 (14.47)	10 (31.25)		
≤66,054.70	65 (85.53)	22 (68.75)		
PE (au)			χ^2=0.72	0.40
≤38,933.21	8 (10.53)	6 (18.75)		
>38,933.21	68 (89.47)	26 (81.25)		
WiAUC (au)			χ^2=10.88	<0.001
≤1,260,081.63	74 (97.37)	24 (75.00)		
>1,260,081.63	2 (2.63)	8 (25.00)		

Table 1 (*continued*)

Table 1 (*continued*)

Variables	NCLNM (n=76)	CLNM (n=32)	Statistic	P
RT (s)			χ^2=1.46	0.23
>3.10	52 (68.42)	18 (56.25)		
≤3.10	24 (31.58)	14 (43.75)		
mTTl (s)			χ^2=6.49	0.01
>25.45	25 (32.89)	3 (9.38)		
≤25.45	51 (67.11)	29 (90.62)		
TTP (s)			χ^2=0.47	0.50
>10.66	29 (38.16)	10 (31.25)		
≤10.66	47 (61.84)	22 (68.75)		
WiR (au)			χ^2=17.52	<0.001
≤101,887.21	65 (85.53)	15 (46.88)		
>101,887.21	11 (14.47)	17 (53.12)		
WiPI (au)			χ^2=6.14	0.01
≤156,760.13	64 (84.21)	20 (62.50)		
>156,760.13	12 (15.79)	12 (37.50)		
WoAUC (au)			χ^2=17.04	<0.001
≤1,675,665.75	76 (100.00)	24 (75.00)		
>1,675,665.75	0 (0.00)	8 (25.00)		
WiWoAUC (au)			χ^2=11.04	<0.001
≤2,935,747.5	75 (98.68)	25 (78.12)		
>2,935,747.5	1 (1.32)	7 (21.88)		
FT (s)			χ^2=0.72	0.40
≤3.77	8 (10.53)	6 (18.75)		
>3.77	68 (89.47)	26 (81.25)		
WoR (au)			χ^2=4.35	0.04
≤41,879.95	58 (76.32)	18 (56.25)		
>41,879.95	18 (23.68)	14 (43.75)		

Data are presented as mean ± standard deviation or n (%). au, arbitrary unit; CLNM, cervical lymph node metastasis; CDFI, color Doppler flow imaging; ETE, extrathyroidal extension; FT, fall time; mTTl, mean transit time local; PE, peak enhancement; RT, rise time; TPO-Ab, thyroid peroxidase antibody; TG-Ab, thyroglobulin antibody; TR-Ab, thyrotropin receptor antibody; TSH, thyroid-stimulating hormone; TTP, time to peak; WiAUC, wash-in area under the curve; WiPI, wash-in perfusion index; WiR, wash-in rate; WoAUC, wash-out area under the curve; WiWoAUC, combined wash-in and wash-out area under the curve; WoR, wash-out rate.

coefficients, signifying their significance in predicting CLNM in PTC patients (*Figure 2*). Subsequently, multivariable logistic regression analysis was employed to develop three predictive models by incorporating the selected features: TR-Ab, TG-Ab, ETE, enhancement defects, mTTl, and WiR (*Table 2*). These models included the clinical model (Model 1), comprising TR-Ab and TG-Ab; the Clinical and US model (Model 2), consisting of ETE, enhancement defects, TR-Ab, and TG-Ab; and the combined model (Model 3), which integrated the clinical

Table 2 Results of multivariable logistic regression analysis in the training sets

Variables	β	SE	Z	P	OR (95% CI)
Intercept	−8.96	2.18	−4.10	<0.001	0.00 (0.00–0.01)
TG-Ab (IU/mL)					
≤60					1.00 (reference)
>60	2.50	1.08	2.33	0.02	12.22 (1.48–100.68)
TR-Ab (IU/mL)					
≤1.75					1.00 (reference)
>1.75	2.99	0.89	3.37	<0.001	19.91 (3.49–113.60)
ETE					
No					1.00 (reference)
Yes	3.76	1.09	3.46	<0.001	42.76 (5.08–359.86)
Filling defects					
Absent					1.00 (reference)
Present	3.64	1.25	2.91	0.004	38.19 (3.28–444.80)
mTTl (s)					
>25.45					1.00 (reference)
≤25.45	2.38	1.13	2.10	0.04	10.78 (1.17–99.00)
WiR (au)					
≤101,887.21					1.00 (reference)
>101,887.21	1.90	0.84	2.27	0.02	6.69 (1.29–34.61)
WoAUC (au)					
≤1,675,665.75					1.00 (reference)
>1,675,665.75	20.32	1683.73	0.01	0.99	666387180.04 (0.00–Inf)
Lesion size	0.02	0.08	0.31	0.76	1.02 (0.88–1.19)

au, arbitrary unit; CI, confidence interval; ETE, extrathyroidal extension; mTTl, mean transit time local; OR, odds ratio; SE, standard error; TG-Ab, thyroglobulin antibody; TR-Ab, thyrotropin receptor antibody; WiR, wash-in rate; WoAUC, wash-out area under the curve.

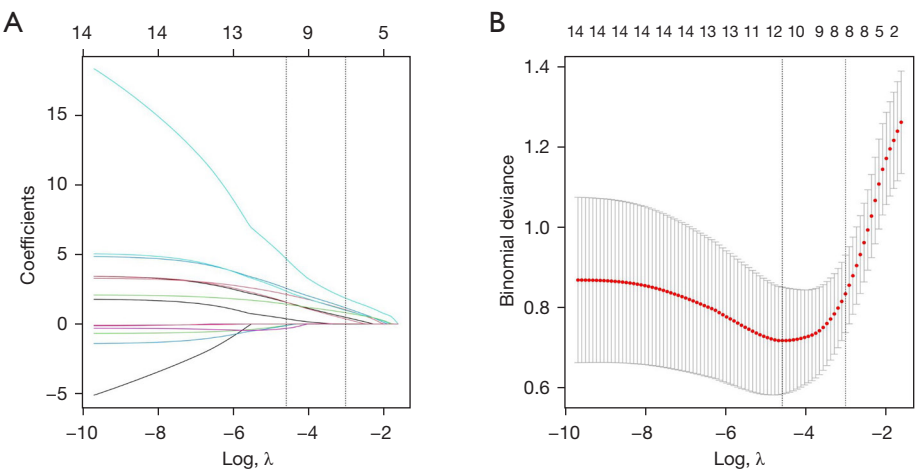

Figure 2 Feature selection using the LASSO method in the training set. LASSO, least absolute shrinkage and selection operator.

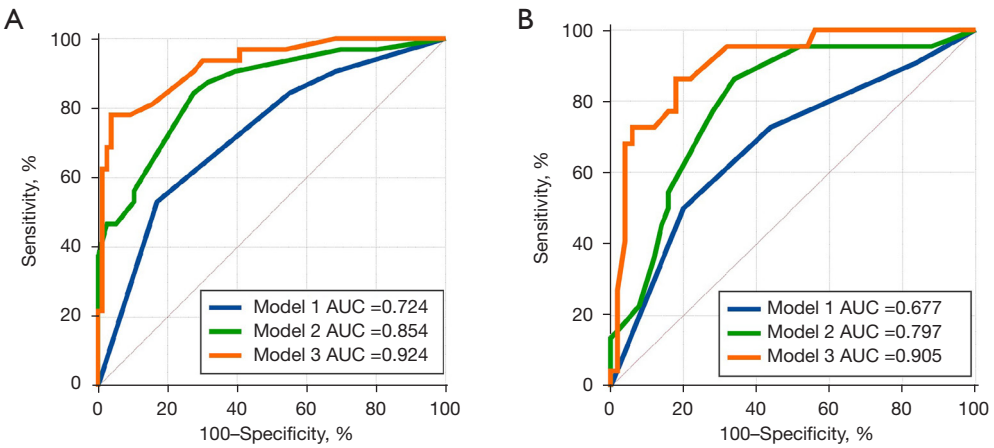

Figure 3 ROC curves of three models in the training (A) and validation (B) sets. AUC, area under the curve; ROC, receiver operating characteristic.

Table 3 Comparison of AUCs of each model for predicting CLNM in PTC patients with HT in the training and validation cohorts

Model	Training cohort		Validation cohort	
	AUC	P value	AUC	P value
Model 1 *vs*. Model 2	0.724 *vs*. 0.854	0.008	0.677 *vs*. 0.797	0.048
Model 1 *vs*. Model 3	0.724 *vs*. 0.924	<0.001	0.677 *vs*. 0.905	0.001
Model 2 *vs*. Model 3	0.854 *vs*. 0.924	0.01	0.797 *vs*. 0.905	0.03

Model 1, incorporating clinical factors; Model 2, integrating clinical and ultrasound factors; Model 3, a combined model that included both clinical and ultrasound factors using DCE-US. AUC, area under the curve; CLNM, cervical lymph node metastasis; DCE-US, dynamic contrast-enhanced ultrasound; HT, Hashimoto's thyroiditis; PTC, papillary thyroid carcinoma.

and US models with DCE-US (*Figure 3*).

The predictive performances of the models are presented in *Table 3*, and the ROC curves are illustrated in *Figure 3*. In the training set, the combined model demonstrated a AUC of 0.924 (95% CI: 0.857–0.966), outperforming both the clinical model with an AUC of 0.724 (95% CI: 0.630–0.806) and the clinical–ultrasound model with an AUC of 0.854 (95% CI: 0.773–0.915). In the training set, the combined model achieved a sensitivity, specificity, and accuracy of 78.12 %, 96.05%, and 88.89 %, respectively. The validation set showed a sensitivity of 86.36%, specificity of 82.00%, and accuracy of 87.50%. The results align with the data presented in *Table 4*.

The DeLong test confirmed that the combined model significantly outperformed the clinical and clinical-ultrasound models in both the training and validation cohorts (P<0.05, *Table 3*). Specifically, in the training cohort, substantial differences in AUC values were observed: 0.924 *vs.* 0.724 (P<0.001) and 0.924 *vs.* 0.854 (P<0.001). Similarly, in the validation cohort, statistically significant differences were detected: 0.905 *vs.* 0.677 (P=0.002) and 0.905 *vs.* 0.797 (P=0.03). These results suggest that DCE-US parameters (mTTl and WiR) may be significant predictors of lymph node status.

Furthermore, Model 2 exhibited a significantly better discriminatory capacity than Model 1 in both the training (AUC 0.854 *vs.* 0.724, P=0.008) and the validation cohort (0.797 *vs.* 0.677, P=0.048, *Table 3*). This indicates that ultrasound factors may serve as valuable markers for predicting CLNM in patients with PTC and HT. These findings are consistent with the data in *Table 3*.

Construction and validation of nomogram

A nomogram was constructed from the combined model in the training set to visualize the prediction results and the contribution of each factor (*Figure 4*). The calibration curves of the nomogram indicated a high concordance between the predicted and actual probabilities of CLNM in both the training and validation cohorts (*Figure 5A*,*5B*).

Table 4 Diagnostic performance of different models in training and validation sets

Cohort	Cut-off value	AUC (95% CI)	Sensitivity, % (95% CI)	Specificity, % (95% CI)	Accuracy, % (95% CI)
Training cohort (n=108)					
Model 1	0.275	0.724 (0.630–0.806)	53.13 (34.7–70.9)	82.89 (72.5–90.6)	74.07 (65.8–82.0)
Model 2	0.157	0.854 (0.773–0.915)	84.37 (67.2–94.7)	72.37 (60.9–82.0)	79.63 (70.8–86.8)
Model 3	0.458	0.924 (0.857–0.966)	78.12 (60.0–90.7)	96.05 (88.9–99.2)	88.89 (81.4–94.1)
Validation cohort (n=72)					
Model 1	0.341	0.677 (0.557–0.783)	50.00 (28.2–71.8)	80.00 (66.3–90.00)	70.83 (58.9–81.0)
Model 2	0.218	0.797 (0.683–0.883)	86.36 (65.1–97.1)	66.00 (51.2–78.8)	73.61 (61.9–83.3)
Model 3	0.273	0.905 (0.813–0.962)	86.36 (65.1–97.1)	82.00 (68.6–91.4)	87.50 (77.6–94.1)

Model 1, incorporating clinical factors; Model 2, integrating clinical and ultrasound factors; Model 3, a combined model that included both clinical and ultrasound factors using DCE-US. AUC, area under the curve; CI, confidence interval; DCE-US, dynamic contrast-enhanced ultrasound.

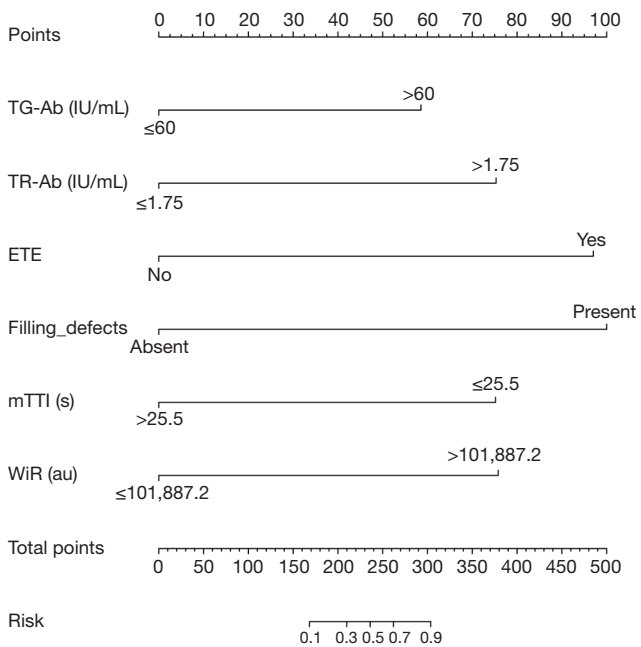

Figure 4 Nomogram for the Model 3 of CLNM. CLNM, cervical lymph node metastasis; ETE, extrathyroidal extension; mTTl, mean transit time local; TG-Ab, thyroglobulin antibody; TR-Ab, thyrotropin receptor antibody; WiR, wash-in rate.

The Hosmer-Lemeshow test further confirmed the model's good fit, with P values of 0.8502 in the training set and 0.7025 in the validation set. Additionally, DCA showed that Model 3 added more net benefits in predicting CLNM than Models 1 and 2, indicating that our developed nomogram based on Model 3 was a valuable method to solve the actual difficulty of predicting CLNM for clinicians in a real-world clinical diagnosis (*Figure 5C,5D*).

Discussion

The association between HT and PTC is complex (21). HT is regarded as both a risk factor for the development of PTC (22,23) and a protective factor for PTC prognosis (24,25). HT-induced inflammation may result in thyroid fibrosis and atrophy, thereby hindering lymphatic dissemination and decreasing the probability of CLNM by compromising adjacent lymphatic arteries. Consequently, PTC patients with concomitant HT may exhibit improved prognosis and disease-free survival (26,27). Paradoxically, although having a more favorable prognosis, these patients frequently undergo more extensive cervical compartment neck dissection and lymphadenectomy than those with PTC alone (28).

Currently, identifying PTC patients with HT at risk for CLNM is challenging due to the lack of dependable diagnostic blood indicators and inadequate thyroid ultrasound imaging. Conversely, predictive variables typically depend on individual assessments, whereas disease prognosis is frequently influenced by factors imperceptible to human observation (29). Unlike other investigations, our predictive model integrated DCE-US, which has garnered considerable interest in the medical field. TICs produced by DCE-US can visibly depict nodule perfusion. Quantitative parameters produced from these curves yield objective data regarding blood perfusion and washout on CEUS, which can be more readily acquired and evaluated by operators,

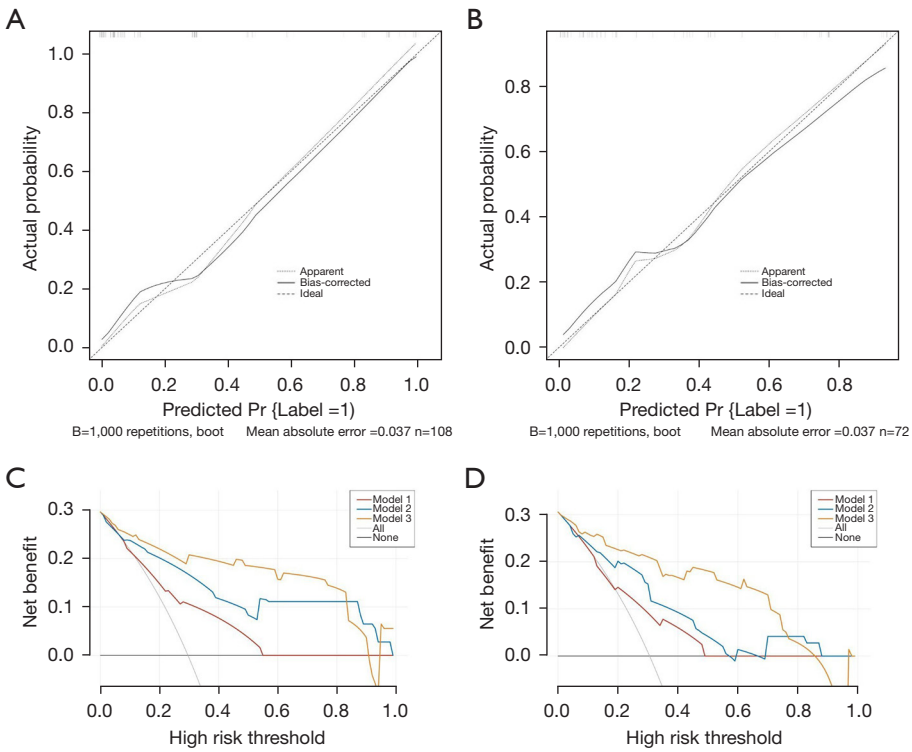

Figure 5 Efficacy of the Model 3 in PTC patients with HT. (A,B) Calibration curves of the Model 3 for predicting CLNM in PTC patients with HT in the training and validation sets. (C,D) Decision curves of three models for predicting CLNM in the training and validation sets. CLNM, cervical lymph node metastasis; HT, Hashimoto's thyroiditis; PTC, papillary thyroid carcinoma.

irrespective of their level of expertise. Consequently, the formulation of an integrated model utilizing clinical data and DCE-US is advantageous in clinical practice.

Thyroid peroxidase antibody (TPO-Ab) and thyroglobulin antibody (TG-Ab) are autoantibodies that specifically target thyroid antigens and are essential clinical markers for HT, with prevalence rates of approximately 75% and 90% in patients with HT, respectively (30). Consistent with the study by Januś *et al.*, no significant connections were observed between the two groups for TPO-Ab (P=0.08) in PTC patients with HT (31). Weng *et al.* investigated the significance of TG-Ab levels in CLNM in patients with differentiated thyroid cancer, indicating that preoperative TG-Ab levels serve as a protective predictor of CLNM (32), corroborating our findings (P=0.01). Our analysis also identified TR-Ab, a form of thyroid-stimulating hormone receptor capable of converting to stimulating and blocking antibodies, as an independent predictor. This antibody was detected in PTC cells of patients with HT and played a crucial role in the occurrence, progression, and immune evasion of PTC. Our findings revealed a negative correlation between TRAb and CLNM (P=0.009), which is consistent with the results reported by Weng *et al.* (32).

Additionally, our study sheds light on the relationship between ultrasound features and CLNM. We evaluated both BMUS and CEUS, with the latter providing information on lesion perfusion (33). CEUS, an innovative imaging technique, has recently garnered considerable attention for its application in thyroid lesions. This non-invasive method allows real-time visualization of blood flow in lesions, enhancing our ability to accurately characterize tumor vascular features and effectively differentiate between benign and malignant growths (34). A recent study has demonstrated the efficacy of this method in identifying metastatic lymph nodes. This research underscored the significance of ETE and enhancement defects as critical indicators of CLNM (35). Our findings revealed that CLNM was more common in patients with ETE and enhancement defects. Lesions displaying ETE and enhancement defects likely indicate a more aggressive tumor behavior, collectively increasing the metastatic potential and possibly facilitating lymphatic spread (36). Moreover,

a previous study indicated that quantitative measures are beneficial for distinguishing between benign and malignant TNs. The study identified the perfusion time parameter mTTl in individuals with CLNM as significant, indicating a reduced overall perfusion time within the lesion, which may be attributable to a decreased blood supply (37). Our investigation demonstrated that accelerated mTTl in initial lesions constituted a risk factor for CLNM in patients, corroborating the results of Kong *et al.*, who reported that mTTl may occur throughout the entire process in patients with CLNM (38). This finding reveals a heterogeneous spatial pattern of tumor blood vessels, a characteristic that plays a pivotal role in driving tumor progression (39). The study indicated that elevated WiR readings signify an increased risk of CLNM in PTC patients with HT. These results align with those of Huang *et al.* (15), who indicated that quantitative CEUS characteristics offer valuable supplementary information beyond subjective human visual and qualitative diagnostic criteria.

To evaluate the predictive value of different data modalities, we developed three distinct models: one based solely on clinical data, a second incorporating both clinical and ultrasound data, and a third integrating clinical, ultrasound, and DCE-US data. The clinical-only and clinical-ultrasound models demonstrated moderate performance, achieving AUCs of 0.738 and 0.863 in the training cohort and 0.730 and 0.817 in the validation cohort, respectively. In contrast, the comprehensive model, which incorporated DCE-US information, exhibited superior performance, with AUCs of 0.925 and 0.915 in the training and validation sets, respectively. This performance marginally surpassed that of the clinical ultrasound and clinical-only models. DCA further corroborated these findings, demonstrating that the integrated model significantly improved the prediction of lymph node metastasis compared to the other two models. These results suggest that the utilization of VueBox® perfusion analysis to extract ultrasound parameters from DCE-US images offers a tangible benefit in predicting CLNM in patients with PTC and HT, potentially informing novel treatment strategies.

There are several limitations in this study. First, as a retrospective study with a limited sample size, selection bias was inevitable. Extensive prospective research using standardized methodologies is essential to corroborate these findings and provide more robust data. The absence of standardization of DCE-US across various manufacturers constrains the generalizability of our findings. This study exclusively examined unifocal PTC; however, multifocal PTCs are recognized risk factors for CLNM and require further investigation. Finally, our study focused solely on TNs and lacked a comparative analysis of the ultrasound characteristics of cervical lymph nodes with and without metastasis, indicating the need for further investigation in this domain.

Conclusions

In conclusion, the present study indicates that the VueBox® is an effective instrument for assessing the dynamic microvascularization of TNs. DCE-US employing VueBox® perfusion analysis can enhance the prediction of CLNM in PTC patients with HT. The integration of clinical information with DCE-US can yield superior diagnostic efficacy for detecting CLNM in these individuals.

Acknowledgments

None.

Footnote

Reporting Checklist: The authors have completed the TRIPOD reporting checklist. Available at https://gs.amegroups.com/article/view/10.21037/gs-2024-510/rc

Data Sharing Statement: Available at https://gs.amegroups.com/article/view/10.21037/gs-2024-510/dss

Peer Review File: Available at https://gs.amegroups.com/article/view/10.21037/gs-2024-510/prf

Funding: This work was partially supported by the Postgraduate Research & Practice Innovation Program of Jiangsu Province (No. SJCX24_1823), Suzhou Clinical Key Diseases Diagnosis and Treatment Technology Special Project (No. LCZX202104), The First Affiliated Hospital of Soochow University Natural Science Foundation Bo Xi Cultivation Program (No. BXQN202235), and The First Affiliated Hospital of Soochow University Bo Xi Clinical Research Project (No. BXLC002).

Conflicts of Interest: All authors have completed the ICMJE uniform disclosure form (available at https://gs.amegroups.com/article/view/10.21037/gs-2024-510/coif). The authors have no conflicts of interest to declare.

Ethical Statement: The authors are accountable for all

aspects of the work in ensuring that questions related to the accuracy or integrity of any part of the work are appropriately investigated and resolved. The study was conducted in accordance with the Declaration of Helsinki (as revised in 2013). The First Affiliated Hospital of Soochow University granted approval for this study (No. 2025227). Owing to the retrospective nature of the study, the requirement for informed consent was waived.

References

1. Jankovic B, Le KT, Hershman JM. Clinical Review: Hashimoto's thyroiditis and papillary thyroid carcinoma: is there a correlation? J Clin Endocrinol Metab 2013;98:474-82.
2. Caturegli P, De Remigis A, Rose NR. Hashimoto thyroiditis: clinical and diagnostic criteria. Autoimmun Rev 2014;13:391-7.
3. Chen S, Niu C, Peng Q, et al. Sonographic Characteristics of Papillary Thyroid Carcinoma With Coexistent Hashimoto's Thyroiditis in the Preoperative Prediction of Central Lymph Node Metastasis. Front Endocrinol (Lausanne) 2021;12:556851.
4. Vita R, Ieni A, Tuccari G, et al. The increasing prevalence of chronic lymphocytic thyroiditis in papillary microcarcinoma. Rev Endocr Metab Disord 2018;19:301-9.
5. Zhao H, Li H. Meta-analysis of ultrasound for cervical lymph nodes in papillary thyroid cancer: Diagnosis of central and lateral compartment nodal metastases. Eur J Radiol 2019;112:14-21.
6. Chen J, Li XL, Zhao CK, et al. Conventional Ultrasound, Immunohistochemical Factors and BRAF(V600E) Mutation in Predicting Central Cervical Lymph Node Metastasis of Papillary Thyroid Carcinoma. Ultrasound Med Biol 2018;44:2296-306.
7. Liu Y, Lv H, Zhang S, et al. The Impact of Coexistent Hashimoto's Thyroiditis on Central Compartment Lymph Node Metastasis in Papillary Thyroid Carcinoma. Front Endocrinol (Lausanne) 2021;12:772071.
8. Zhao D, Li W, Zhang X. Development and validation of a nomogram for preoperative prediction of ipsilateral cervical central lymph node metastasis in papillary thyroid cancer: a population-based study. Gland Surg 2024;13:528-39.
9. Kim SS, Lee BJ, Lee JC, et al. Coexistence of Hashimoto's thyroiditis with papillary thyroid carcinoma: the influence of lymph node metastasis. Head Neck 2011;33:1272-7.
10. Miao H, Zhong J, Xing X, et al. A nomogram based on the risk factors of cervical lymph node metastasis in papillary thyroid carcinoma coexistent with Hashimoto's thyroiditis. Clin Hemorheol Microcirc 2023;85:235-47.
11. Zhao W, You L, Hou X, et al. The Effect of Prophylactic Central Neck Dissection on Locoregional Recurrence in Papillary Thyroid Cancer After Total Thyroidectomy: A Systematic Review and Meta-Analysis : pCND for the Locoregional Recurrence of Papillary Thyroid Cancer. Ann Surg Oncol 2017;24:2189-98.
12. Piscaglia F, Nolsøe C, Dietrich CF, et al. The EFSUMB Guidelines and Recommendations on the Clinical Practice of Contrast Enhanced Ultrasound (CEUS): update 2011 on non-hepatic applications. Ultraschall Med 2012;33:33-59.
13. Zhang Y, Luo YK, Zhang MB, et al. Diagnostic Accuracy of Contrast-Enhanced Ultrasound Enhancement Patterns for Thyroid Nodules. Med Sci Monit 2016;22:4755-64.
14. Ma JJ, Ding H, Xu BH, et al. Diagnostic performances of various gray-scale, color Doppler, and contrast-enhanced ultrasonography findings in predicting malignant thyroid nodules. Thyroid 2014;24:355-63.
15. Huang Y, Wang Y, Liu L, et al. VueBox® perfusion analysis of dynamic contrast enhanced ultrasound provides added value in the diagnosis of small thyroid nodules. Clin Hemorheol Microcirc 2023;83:409-20.
16. Zhou BY, Liu H, Pu YY, et al. Quantitative analysis of pre-treatment dynamic contrast-enhanced ultrasound for assessing the response of colorectal liver metastases to chemotherapy plus targeted therapy: a dual-institutional study. Abdom Radiol (NY) 2024;49:414-24.
17. Dong Y, Chen S, Möller K, et al. Applications of Dynamic Contrast-Enhanced Ultrasound in Differential Diagnosis of Hepatocellular Carcinoma and Intrahepatic Cholangiocarcinoma in Non-cirrhotic Liver. Ultrasound Med Biol 2023;49:1780-8.
18. Wiesinger I, Kroiss E, Zausig N, et al. Analysis of arterial dynamic micro-vascularization with contrast-enhanced ultrasound (CEUS) in thyroid lesions using

external perfusion software: First results. Clin Hemorheol Microcirc 2016;64:747-55.
19. Zhou J, Yin L, Wei X, et al. 2020 Chinese guidelines for ultrasound malignancy risk stratification of thyroid nodules: the C-TIRADS. Endocrine 2020;70:256-79.
20. Platz Batista da Silva N, Jung EM, Jung F, et al. VueBox® perfusion analysis of contrast-enhanced ultrasound (CEUS) examinations in patients with primary hyperparathyroidism for preoperative detection of parathyroid gland adenoma. Clin Hemorheol Microcirc 2018;70:423-31.
21. Del Rio P, Cataldo S, Sommaruga L, et al. The association between papillary carcinoma and chronic lymphocytic thyroiditis: does it modify the prognosis of cancer? Minerva Endocrinol 2008;33:1-5.
22. Le Y, Geng C, Gao X, et al. The risk of thyroid cancer and sex differences in Hashimoto's thyroiditis, a meta-analysis. BMC Endocr Disord 2024;24:151.
23. Kim EY, Kim WG, Kim WB, et al. Coexistence of chronic lymphocytic thyroiditis is associated with lower recurrence rates in patients with papillary thyroid carcinoma. Clin Endocrinol (Oxf) 2009;71:581-6.
24. Xu J, Ding K, Mu L, et al. Hashimoto's Thyroiditis: A "Double-Edged Sword" in Thyroid Carcinoma. Front Endocrinol (Lausanne) 2022;13:801925.
25. Lee JH, Kim Y, Choi JW, et al. The association between papillary thyroid carcinoma and histologically proven Hashimoto's thyroiditis: a meta-analysis. Eur J Endocrinol 2013;168:343-9.
26. Medas F, Canu GL, Cappellacci F, et al. Prophylactic Central Lymph Node Dissection Improves Disease-Free Survival in Patients with Intermediate and High Risk Differentiated Thyroid Carcinoma: A Retrospective Analysis on 399 Patients. Cancers (Basel) 2020;12:1658.
27. Jara SM, Carson KA, Pai SI, et al. The relationship between chronic lymphocytic thyroiditis and central neck lymph node metastasis in North American patients with papillary thyroid carcinoma. Surgery 2013;154:1272-80; discussion 1280-2.
28. Lai V, Yen TW, Rose BT, et al. The Effect of Thyroiditis on the Yield of Central Compartment Lymph Nodes in Patients with Papillary Thyroid Cancer. Ann Surg Oncol 2015;22:4181-6.
29. Jin P, Chen J, Dong Y, et al. Ultrasound-based radiomics nomogram combined with clinical features for the prediction of central lymph node metastasis in papillary thyroid carcinoma patients with Hashimoto's thyroiditis. Front Endocrinol (Lausanne) 2022;13:993564.
30. Mikulska AA, Karaźniewicz-Łada M, Filipowicz D, et al. Metabolic Characteristics of Hashimoto's Thyroiditis Patients and the Role of Microelements and Diet in the Disease Management-An Overview. Int J Mol Sci 2022;23:6580.
31. Januś D, Wójcik M, Taczanowska-Niemczuk A, et al. Ultrasound, laboratory and histopathological insights in diagnosing papillary thyroid carcinoma in a paediatric population: a single centre follow-up study between 2000-2022. Front Endocrinol (Lausanne) 2023;14:1170971.
32. Weng L. Role of ultrasound guided fine needle aspiration cytology combined with thyroid peroxidase and thyroglobulin antibodies in evaluating cervical lymph node metastasis in thyroid cancer. Oncol Lett 2024;28:512.
33. Tessler FN, Middleton WD, Grant EG. Thyroid Imaging Reporting and Data System (TI-RADS): A User's Guide. Radiology 2018;287:1082. Erratum for: Radiology 2018;287:29-36.
34. Ruan J, Xu X, Cai Y, et al. A Practical CEUS Thyroid Reporting System for Thyroid Nodules. Radiology 2022;305:149-59.
35. Xiang D, Hong Y, Zhang B, et al. Contrast-enhanced ultrasound (CEUS) facilitated US in detecting lateral neck lymph node metastasis of thyroid cancer patients: diagnosis value and enhancement patterns of malignant lymph nodes. Eur Radiol 2014;24:2513-9.
36. Li QL, Ma T, Wang ZJ, et al. The value of contrast-enhanced ultrasound for the diagnosis of metastatic cervical lymph nodes of papillary thyroid carcinoma: A systematic review and meta-analysis. J Clin Ultrasound 2022;50:60-9.
37. Gu F, Han L, Yang X, et al. Value of time-intensity curve analysis of contrast-enhanced ultrasound in the differential diagnosis of thyroid nodules. Eur J Radiol 2018;105:182-7.
38. Kong Q, Yu Y, Qian Q, et al. Clinical value of ultrasound parameters PI, TTP, and MTT in assessing cervical lymph node metastasis of papillary thyroid carcinoma. Am J Transl Res 2024;16:809-16.
39. Rajabi S, Dehghan MH, Dastmalchi R, et al. The roles and role-players in thyroid cancer angiogenesis. Endocr J 2019;66:277-93.

Cite this article as: Zhang K, Zhao D, Song Y, Wu X, Jin C, Dong F. Value of dynamic contrast-enhanced ultrasound in predicting cervical lymph node metastasis in papillary thyroid carcinoma patients with Hashimoto's thyroiditis. Gland Surg 2025;14(4):597-610. doi: 10.21037/gs-2024-510